



**HAL**  
open science

## Experimental evidence for calcium-chloride ion pairs in the interlayer of montmorillonite. A XRD profile modeling approach.

Eric Ferrage, Christophe Tournassat, Emmanuel Rinnert, Laurent Charlet,  
Bruno Lanson

### ► To cite this version:

Eric Ferrage, Christophe Tournassat, Emmanuel Rinnert, Laurent Charlet, Bruno Lanson. Experimental evidence for calcium-chloride ion pairs in the interlayer of montmorillonite. A XRD profile modeling approach.. *Clays and Clay Minerals*, 2005, 53, pp.348-360. 10.1346/CCMN.2005.0530403 . hal-00105762

**HAL Id: hal-00105762**

**<https://hal.science/hal-00105762v1>**

Submitted on 12 Oct 2006

**HAL** is a multi-disciplinary open access archive for the deposit and dissemination of scientific research documents, whether they are published or not. The documents may come from teaching and research institutions in France or abroad, or from public or private research centers.

L'archive ouverte pluridisciplinaire **HAL**, est destinée au dépôt et à la diffusion de documents scientifiques de niveau recherche, publiés ou non, émanant des établissements d'enseignement et de recherche français ou étrangers, des laboratoires publics ou privés.

# Experimental evidence for calcium-chloride ion pairs in the interlayer of montmorillonite. A XRD profile modeling approach

Eric Ferrage<sup>1,2,\*</sup>, Christophe Tournassat<sup>2,3</sup>, Emmanuel Rinnert<sup>2,4</sup>, Laurent Charlet<sup>1</sup>, Bruno Lanson<sup>1</sup>

<sup>1</sup> Environmental Geochemistry Group, LGIT, CNRS – Joseph Fourier University, P.O. Box 53, 38041 Grenoble, France

<sup>2</sup> ANDRA, Parc de la Croix Blanche 1/7 rue Jean Monnet, 92298 Châtenay-Malabry Cedex, France

<sup>3</sup> BRGM, 3 avenue Claude Guillemin, 45060 Orléans Cedex 2, France

<sup>4</sup> Laboratoire de Chimie Physique et Microbiologie pour l'Environnement, UMR 7564 CNRS- Université Henri Poincaré, 405 rue de Vandoeuvre, 54600 Villers-Lès-Nancy, France.

\*Corresponding author: [eric.ferrage@obs.ujf-grenoble.fr](mailto:eric.ferrage@obs.ujf-grenoble.fr) - Address: Environmental Geochemistry Group, LGIT, CNRS – Joseph Fourier University, P.O. Box 53, 38041 Grenoble, France

Keywords: montmorillonite, ion pairs, XRD profile modeling.

## ABSTRACT

Montmorillonite was equilibrated with high normality  $\text{Cl}^-$  solutions to assess the possible presence of  $\text{MeCl}^+$  ion pairs in smectite interlayers which is suggested by chemical modeling of cation exchange experimental studies. Structural modifications induced by the presence of such ion pairs, and more especially those related to smectite hydration properties, were characterized from the modeling of experimental X-ray diffraction (XRD) profiles. As compared to those obtained from samples prepared at low ionic strength, XRD patterns from samples equilibrated in high ionic strength  $\text{CaCl}_2$  solutions exhibited a small positional shift of 00 $l$  basal reflections indicating a higher layer thickness. Rationality of basal reflection positions is also improved and the width of these reflections is decreased. These qualitative modifications are related to the existence of a more homogeneous hydration state with the sole presence at 40% relative humidity (RH) of bi-hydrated smectite layers (2W layers) in high ionic strength samples. By contrast, layers with contrasting hydration states coexist in samples prepared at low ionic strength. The stability of this homogeneous 2W hydration state is also extended toward low RH values in the sample prepared at high ionic strength.

In addition, the intensity distribution is modified in samples prepared at high ionic strength as compared to those obtained at low ionic strength. In particular the relative intensity of the (002) reflection is strongly enhanced in the former samples. This modification arises from an increased electron density in the interlayer mid-plane of 2W layers which is best explained by the presence of cation – chloride ion pairs replacing the divalent cations occupying this structural position in low ionic strength samples. The increased amounts of interlayer species (ion pairs and  $\text{H}_2\text{O}$  molecules), which are confirmed by near infrared diffuse reflectance spectroscopy results, and the larger size of  $\text{CaCl}^+$  pairs as compared to

Ca<sup>2+</sup> cations lead to a more stable layer thickness most probably as a result of decreased layer corrugation. Consistent results were obtained for Sr and Mg cations.

## INTRODUCTION

Bentonite, a clay material mainly constituted of smectite, is considered a potential engineered barrier material for nuclear waste disposal. In high- and intermediate-level long-lived radioactive wastes (ILLW wastes) disposal sites, one possible disposal method involves indeed vitrified waste placed in containers and overpacks, encased in exogenous materials (near-field engineered barrier) and buried in a clay-rich geological formation (far-field barrier). The potential of smectite as near- to far-field barrier material arises from the combination of mechanical self-healing ability, low hydraulic conductivity and high sorption capacities. The latter feature is expected to prevent or to delay radionuclide migration. However, the initial properties of smectite could be significantly altered as a consequence of storage-induced perturbations. For example, the use of concrete for waste overpacks or the oxidation of pyrite, which is often present as an accessory mineral in the geological environment, can induce a wide pH-range in solutions in contact with the clay barriers. In turn such perturbations of the solution chemistry may lead to structural changes affecting both the geological host formation and the engineered clay barrier.

An octahedral sheet sandwiched by two tetrahedral sheets builds up smectite layers. Substitutions in either tetrahedral or octahedral sites induce a permanent negative layer charge, balanced by the presence of hydrated interlayer cations. The relationship between interlayer cation composition and the composition of the solution in contact with clay surfaces has been studied for decades, and cation exchange thermodynamics has been developed to model the composition in the clay interlayers (Vanselow, 1932a; Sposito, 1977, 1981, 1984;

Elprince *et al.*, 1980; Shainberg *et al.*, 1980; Sposito *et al.*, 1981; Fletcher and Sposito, 1989 and references therein). In the 1980's, Sposito *et al.* (1983a, 1983b) first suspected the sorption of cation – chloride ion pairs from the comparison between Mg-Na and Ca-Na exchange experiments performed in perchlorate and chloride anionic backgrounds. High exchange selectivity coefficients were found for these complex monovalent cations as compared to simple monovalent cations (Fletcher and Sposito, 1989). The relevance of this cation – anion – clay interaction model was further assessed by various exchange experiments (Suarez and Zahow, 1989; Rhue and Reve, 1990) producing conflicting data and various conceptual models. Despite a detailed analysis of the source of apparent conflicts between these data (Sposito, 1991), owing principally to experimental conditions such as clay content, cation – chloride ion pairs are usually not considered in thermodynamic exchange calculations. Sorption of cation – chloride ion pairs in the interlayer of clay minerals was confirmed recently from cation exchange experiments (Tournassat *et al.*, 2004a, 2004b) and from the modeling of the interlayer composition in clay particles equilibrated with seawater (Tournassat *et al.*, 2004b; Charlet and Tournassat, 2005). These authors also suspected the presence of  $\text{CaOH}^+$  ion pairs as exchangeable cation at high pH. Similarly, recent studies by nuclear magnetic resonance have revealed the coexistence of  $\text{Cd}^{2+}$  and  $\text{CdCl}^+$  in the interlayers of smectites equilibrated in high-concentration cadmium chloride solutions (Di Leo and O' Brien, 1999; Di Leo and Cuadros, 2003). However, the location of sorbed cation – chloride and cation – hydroxide ion pairs were not readily identified by spectroscopy or diffraction methods as opposed to other cations (Hyun *et al.*, 2000; Schlegel *et al.*, 2001).

The impact of smectite interlayer composition on smectite hydration has been extensively studied using X-ray diffraction (XRD) from the positions of (00 $\ell$ ) basal reflections. With increasing moisture in its environment, smectite expands in different steps, corresponding to the intercalation of 0, 1, 2 or 3 sheets of  $\text{H}_2\text{O}$  molecules in the interlayer

(Nagelschmidt, 1936; Bradley *et al.*, 1937; Mooney *et al.*, 1952; Norrish, 1954; Walker, 1956). From these pioneer studies, it is now commonly accepted that the expandability of 2:1 phyllosilicates is controlled by factors such as the nature of interlayer cations, the layer charge and its location (octahedral vs. tetrahedral). These general observations have led to different models in which crystalline swelling is controlled by a balance between the repulsive forces due to 2:1 layers interactions and the attractive forces between hydrated interlayer cations and the negatively charged surface of siloxane layers (Norrish, 1954; Van Olphen, 1965; Kittrick, 1969a, 1969b; Laird, 1996, 1999). The development of X-ray diffraction modeling techniques allows these observations to be refined by investigating defective structures such as those resulting from the coexistence of layers having different thicknesses (Ben Brahim *et al.*, 1983, 1984; Bérend *et al.*, 1995; Cases *et al.*, 1997; Cuadros, 1997). Ferrage *et al.* (2005a, 2005b) used a similar modeling approach to determine the hydration properties of montmorillonite and beidellite and observed that (i) the nature of the interlayer cation and its ability to sorb water molecules determines the layer thickness of the bi-hydrated and monohydrated layers and confirmed that (ii) relative proportions of the different layer types, which correspond to different hydration states, are determined by smectite layer charge and charge location.

The present work aims at characterizing the variation of montmorillonite hydration state as a function of the anionic background in order to improve understanding of smectite reactivity in disturbed chemical conditions, such as those expected to occur in near- and/or far-field barriers. From XRD data, the present study focuses on the effect of chloride on Ca-exchanged montmorillonite to assess the presence of cation – chloride ion pairs in the smectite interlayer. Additional near infrared diffuse reflectance spectroscopy data was used to study the local arrangement of H<sub>2</sub>O molecules around interlayer species.

## MATERIALS AND METHODS

### *Sample preparation*

The smectite used for this study is the SWy-2 montmorillonite reference from the Source Clay Repository of The Clay Mineral Society with structural formula (Stucki *et al.*, 1984):  $[(Al_{3.01} Fe_{0.43} Mg_{0.56})(Si_{7.97} Al_{0.03})O_{20}(OH)_4] M^{+}_{0.72}$ . This montmorillonite is originally Na-saturated, and exhibits a low octahedral charge and extremely limited tetrahedral substitutions (Mermut and Lagaly, 2001).

Size fractionation was performed by centrifugation to obtain a suspension of the <2  $\mu m$  size fraction. Ion-exchange processes were achieved on this clay separate at room temperature with 1 mol.L<sup>-1</sup> aqueous saline solutions of MeCl<sub>2</sub> (Me = Ca, Sr or Mg) or of NaCl prepared from analytical grade reagents and deionized water (milli-Q/18.2 M $\Omega$  cm<sup>-1</sup>). SWy-2 suspensions in these saline solutions were shaken mechanically for 24h before separation of the solid fraction by centrifugation and addition of fresh saline solution. These steps were repeated three times to ensure a complete cation exchange. Then MeCl-SWy samples were prepared by direct filtration of the clay suspension whereas for Me-SWy samples, excess salt was washed out by four 24h cycles that included sedimentation, removal of the supernatant and immersion in deionized water.

### *Choice of experimental conditions*

Figure 1 shows the montmorillonite interlayer composition computed as a function of ionic strength in CaCl<sub>2</sub> ion background, according to thermodynamics data reported by Tournassat *et al.* (2004b - Table 1). Simulations were performed using the Phreeqc2 code (Parkhurst and Appelo, 1999) using Vanselow's thermodynamics convention (Vanselow,

1932b) as this versatile computer code is amenable to various conventions used to describe cation exchange. According to Figure 1,  $\text{Ca}^{2+}$  should be the sole calcium interlayer species when the ionic strength value (I) is lower than  $0.01 \text{ mol.L}^{-1}$ , whereas  $\text{CaCl}^+$  presumably becomes the unique interlayer cation when I is higher than  $2 \text{ mol.L}^{-1}$ . Computed interlayer compositions are similar if Sr or Mg are considered instead of Ca. Hence, Me-SWy and MeCl-SWy samples correspond to two ionic strength values for which the predicted interlayer composition of smectite is completely different, *e.g.*, Me-SWy samples (Me = Ca, Sr or Mg) at  $I < 0.01 \text{ mol.L}^{-1}$  and MeCl-SWy samples and  $I = 2.7 \text{ mol.L}^{-1}$  (corresponding to a total normality of  $1 \text{ mol.L}^{-1}$   $\text{MeCl}_2$  solution). Na-SWy and NaCl-SWy samples were prepared following the same procedure.

### *X-ray diffraction*

For XRD analysis, suspension aliquots were poured through a Millipore filter ( $0.4\mu\text{m}$ ) and the resulting clay films were transferred onto a previously weighed glass slide. The oriented preparations obtained were then dried at room temperature and the mass of montmorillonite on the glass slide was measured for the needs of X-ray diffraction modeling. XRD patterns were then recorded using a Bruker D5000 diffractometer equipped with an Ansyco rh-plus 2250 humidity control device coupled to an Anton Paar TTK450 chamber. Experimental measurement parameters were a  $0.04^\circ 2\theta$  step size and 6s counting time per step. The divergence slit, the two Soller slits, antiscatter and resolution slits were  $0.5^\circ$ ,  $2.3^\circ$ ,  $2.3^\circ$ ,  $0.5^\circ$  and  $0.06^\circ$ , respectively.

For each sample, XRD patterns were recorded over a time span that did not exceed two days after glass slide preparation to avoid kinetically driven dehydration of the



montmorillonite. A 15 min waiting period was observed before XRD data collection to ensure hydration equilibration at the desired relative humidity (RH).

### *X-ray diffraction modeling*

Experimental XRD patterns were fitted using a trial-and-error approach and the program initially developed by Drits and Sakharov (1976). Instrumental and experimental factors such as horizontal and vertical beam divergences, goniometer radius, slide length and sample thickness were measured and introduced without further refinement. The linear absorption coefficient ( $\mu^*$ ) and z-coordinates of the 2:1 silicate layer were set as recommended by Moore and Reynolds (1997). The distribution of coherent scattering domain sizes (N) was assumed to be lognormal and characterized by its mean value (Drits *et al.*, 1997b). Sigmastar parameter ( $\sigma^*$ ), which corresponds to the distribution of particle orientation in the sample, was considered as a variable parameter (Moore and Reynolds, 1997). A  $\sigma_z$  parameter, which corresponds to atomic position fluctuations leading to a disorder of the second type (Guinier, 1964; Drits and Tchoubar, 1990), was also refined. This latter parameter can be described as the standard deviation of the layer thickness from a mean value.

The three layer types corresponding to the hydration states reported for montmorillonite in non-saturated conditions are the following: dehydrated (0W) layers with interlayer cations in the interlayer mid-plane, mono-hydrated (1W) layers with interlayer cations and H<sub>2</sub>O molecules in the same central plane, and bi-hydrated (2W) layers with the central cation plane sandwiched between two planes of H<sub>2</sub>O molecules at a distance of 1.2 Å along the c\* axis (Ferrage *et al.*, 2005a). The quality of fit to the experimental patterns was assessed using the Rp parameter (Howard and Preston, 1989). This unweighted parameter was

chosen as being mostly influenced by intense peaks such as the (001) reflection, where most information on the relative proportions of different layer types and on their thickness is concentrated. Calculated XRD patterns are cut at  $\sim 5^\circ 2\theta$  CuK $\alpha$  because of significant background discrepancies over the low-angle region, possibly resulting from an incorrect description of crystalline defects as proposed by Plançon (2002). However, the profiles of the (00 $l$ ) reflections calculated using either model are similar and the low-angle misfit does not challenge the results obtained in the present study (Ferrage *et al.*, 2005a).

### *Near Infrared Diffuse Reflectance analysis*

Near infrared diffuse reflectance (NIR-DR) spectra were recorded using a Perkin Elmer 2000 FTIR spectrometer equipped with a deuterated triglycine sulphate (DTGS) detector, a tungsten-halogen source and a quartz beam-splitter. Spectra were collected using a spectral resolution of  $8\text{ cm}^{-1}$ . The optical device used is based on the Harrick© equipment. Diffuse reflectance spectra were recorded from  $4000$  to  $8000\text{ cm}^{-1}$  as the sum of 50 individual scans. Samples were placed into an Harrick© cell in which temperature and pressure were controlled from  $25^\circ\text{C}$  to  $100^\circ\text{C}$  and from  $10^{-4}$  Pa to  $10^5$  Pa, respectively. Sample temperature was measured by a Pt resistance which allows measurements with an accuracy better than  $0.1^\circ\text{C}$ . Spectra of hydrated samples were first recorded before pumping, when samples were equilibrated with room humidity, which was equal to  $(40 \pm 5)\%$ . Samples were subsequently out-gassed at  $60^\circ\text{C}$  for 16 hours under a residual pressure of  $\sim 5 \cdot 10^{-3}$  Pa and spectra were then recorded at  $25^\circ\text{C}$  under a residual pressure of  $5 \cdot 10^{-4}$  Pa. The reported diffuse reflectance,  $R$ , is defined as:

$$R = -\log \frac{I_s^D(\sigma)}{I_0^D(\sigma)} \quad (1)$$

where  $I_s^D$  is the measured diffused irradiance of the sample,  $I_0^D$  the measured diffused irradiance of the reference, and  $\sigma$  the wavenumber. The reference was taken at 24.8°C from a KBr powder dried under a residual pressure of  $5 \cdot 10^{-3}$  Pa.

For clay samples, the spectral domain presented in this study can be split in two regions. From 4550 to 5500  $\text{cm}^{-1}$ , only  $\text{H}_2\text{O}$  molecules can be observed from the combinations of stretching and bending modes. From 6500 to 7500  $\text{cm}^{-1}$ , overtones of stretching modes of all hydroxyl groups, both from interlayer  $\text{H}_2\text{O}$  molecules and from the silicate framework, are visible (Burneau *et al.*, 1990; Madejova *et al.*, 2000b). In previous IR studies of smectites, fundamental stretching modes have been reported over the 3370-3670  $\text{cm}^{-1}$  range (Madejova *et al.*, 2000b; Vantelon *et al.*, 2001; Bishop *et al.*, 2002). Consequently, the frequency range calculated for the first stretching overtone extends from 6575-7175  $\text{cm}^{-1}$ , with a 82.5  $\text{cm}^{-1}$  anharmonicity coefficient for OH groups (Burneau and Carteret, 2000).

## RESULTS AND DISCUSSION

### *Qualitative description of Me- and MeCl-SWy XRD patterns*

XRD patterns recorded at 40% RH for Ca- and CaCl-SWy samples are shown on Figure 2a, whereas  $d_{(001)}$  values and departure from rationality  $\xi$ , calculated as the standard deviation of  $\ell \times (00\ell)$  values, are reported in Table 2. An increased  $\xi$  parameter is indicative of interstratified structures.

A small shift of the (001) reflection towards lower angles is visible for the XRD pattern of sample CaCl-SWy as compared to sample Ca-SWy, corresponding to a small increase of layer thickness rather than to a lower coherent scattering domain size (CSDS) along the  $c^*$  axis as peak width is lower for sample CaCl-SWy than for sample Ca-SWy. An

intensity increase of (002), (003), (004) and (005) reflections, together with their sharpening, is also visible on the XRD pattern of sample CaCl-SWy as compared to sample Ca-SWy.

Finally, the lower  $\xi$  parameter measured for sample CaCl-SWy indicates a more homogeneous hydration state in this sample as compared to sample Ca-SWy. To verify that the observed modifications are not related to the ionic strength of the suspension, the same experiment was performed on Na-SWy and NaCl-SWy samples and identical XRD patterns, within experimental reproducibility, were obtained for the two samples (Figure 2b, Table 2).

For Mg-, MgCl-, Sr-, and SrCl-SWy samples, observations similar to those reported for Ca- and CaCl-SWy samples were made (Figure 2a). However for sample SrCl-SWy, the presence of SrCl<sub>2</sub> salt precipitation prevents the precise observation of the high angles XRD pattern region. A  $d_{(001)}$  increase is observed from 15.03 Å for sample Mg-SWy to 15.40 Å for sample MgCl-SWy, and from 15.40 Å for sample Sr-SWy to 15.53 Å for sample SrCl-SWy, this increase being systematically associated with a sharpening of the (001) reflection (Table 2 – Figure 2a). In addition, the  $\xi$  parameter decreases for sample SrCl-SWy as compared to sample Sr-SWy, whereas it increases slightly for MgCl-SWy as compared to Mg-SWy (Table 2). However, the  $\xi$  parameters determined for all samples are low (<0.15 Å) implying homogeneous hydration states in all cases. Similar peak positions and  $\xi$  parameters were obtained for Na-SWy and NaCl-SWy samples (Table 2).

#### *Origin of the observed structural changes*

*Hydration homogeneity and layer fluctuation.* To assess further the hydration homogeneity, the full width at half maximum intensity (FWHM) of all measurable (00 $\ell$ ) reflections is plotted as a function of the  $\ell$  index, after correction by a  $\cos\theta$  factor to compensate for particle-size broadening (Figure 3). For a given sample (Me-SWy or MeCl-SWy) all FWHM

values are aligned. If different layer types were interstratified in the samples, such a steady broadening of (00 $\ell$ ) reflections would not be observed. Rather, interstratification of layers exhibiting different layer thickness values as a result of their contrasting hydration states would lead to a random broadening of (00 $\ell$ ) reflections as a function of the  $\ell$  index. For a given (00 $\ell$ ) reflection this broadening can be predicted from Méring's principle (Méring, 1949; Moore and Reynolds, 1997).

The high hydration homogeneity of the different samples deduced from both the low  $\xi$  values and from the linear dependence of (00 $\ell$ ) reflection FWHMs on  $\ell$  index makes it possible to interpret the slopes of the linear correlations shown on Figure 3 as indicative of layer thickness fluctuations. These fluctuations are similar to strains and induce peak broadening of (00 $\ell$ ) reflections steadily increasing with  $\ell$  index (Kodama *et al.*, 1971). The slope of this linear correlation is dramatically decreased for sample CaCl-SWy as compared to sample Ca-SWy, thus indicating a lower layer thickness variability for the former sample. For Mg- and MgCl-SWy samples on the one hand and for Sr- and SrCl-SWy samples on the other, the slopes of the linear correlations are similar even though MgCl- and SrCl-SWy samples have lower FWHM values than the corresponding Mg- and Sr-SWy samples. Similar evolutions of basal reflection FWHM were observed as a function of the  $\ell$  index for Na-SWy and NaCl-SWy samples (Figure 3).

*Distribution of intensity.* Another significant feature of experimental patterns recorded for Me- and MeCl-SWy samples is the intensity modification of (00 $\ell$ ) reflections and especially that of the (002) reflection, which is strongly increased in MeCl-SWy samples as compared to the corresponding Me-SWy samples. As discussed above similar high hydration homogeneity is expected for all samples, and reflection intensity is directly related to the structure factor of the main layer type, which in turn includes the scattering factors of all its constituting atoms.

As a consequence, the structure factor of the different (00 $\ell$ ) reflections and thus their intensity ratio are modified if additional elements are introduced in montmorillonite interlayers. If smectite interlayers incorporate MeCl<sup>+</sup>, the increase in electronic density as compared to interlayer Me<sup>2+</sup> species results both from the presence of Cl<sup>-</sup> anions and from the monovalent character of the MeCl<sup>+</sup> ion pair. As a result, the amount of interlayer species has to be doubled to compensate for the permanent layer charge deficit. The modification of the electronic density resulting from the presence of monovalent ion pairs as compared to divalent cations can be estimated from the number of electrons corresponding to each charge compensating species. Ca<sup>2+</sup> cations hold 18e<sup>-</sup>, that is 9e<sup>-</sup> per charge unit (c.u.). This index ( $\eta$ ) corresponds to the atomic scattering factor for  $\theta=0$  weighted for the cation valency. As Cl<sup>-</sup> anions hold 18e<sup>-</sup>, CaCl<sup>+</sup> ion pairs have 36e<sup>-</sup>/c.u. Similar calculations for other divalent cations lead to the following values:  $\eta\text{Mg}^{2+}=6\text{e}^-/\text{c.u.}$ ,  $\eta\text{MgCl}^+=30\text{e}^-/\text{c.u.}$ ,  $\eta\text{Sr}^{2+}=18\text{e}^-/\text{c.u.}$  and  $\eta\text{SrCl}^+=54\text{e}^-/\text{c.u.}$  In agreement with this basic approach, the integrated intensity ratio between (002)<sub>MeCl<sup>+</sup></sub> and (002)<sub>Me<sup>2+</sup></sub> reflections is linearly correlated to the  $\eta$  ratio between the two compensating species ( $\eta\text{MeCl}^+/\eta\text{Me}^{2+}$  – Figure 4). This correlation suggests the presence of cation – chloride ion pairs in the interlayers of MeCl-SWy samples.

#### *Ca- and CaCl-SWy XRD profile modeling*

The possible presence of CaCl<sup>+</sup> ion pairs in smectite interlayers may be further assessed from the modeling of the whole experimental XRD patterns. For each pattern modeling, two mixed-layer structures (MLSs) that can contain one (periodic structure), two or three layer types (0W, 1W, 2W) randomly interstratified (R=0) were considered to account for the hydration heterogeneity. The presence of two MLSs does not imply that two populations of particles are physically present in the sample. Due to layer charge distribution, the smectite

structure may incorporate layers exhibiting different hydration states as a function of the relative humidity (Ferrage *et al.*, 2005a, 2005b). As a result, special attention was paid to have strictly identical chemical composition and atomic z-coordinates for each layer type, as well as  $\sigma^*$ , and  $\sigma_z$  in the two MLSs.

The strategy used for XRD profile modeling has been to mimic as closely as possible the (001) reflection with a MLS as homogeneous as possible, that is containing as few different layer types as possible. If it proved necessary to obtain a good fit, a second MLS was introduced to fill the gaps between calculated and experimental patterns, and to better account for the hydration heterogeneity of the sample. Finally the structure of the different layer types, and more especially their interlayer structure, was refined to reproduce the intensity distribution over the whole angular range.

*Sample Ca-SWy.* Qualitatively, the XRD pattern of sample Ca-SWy recorded at 40% RH exhibits diffraction maxima forming an almost rational series corresponding to 2W layers. Asymmetries on the high-angle side of the (001) reflection and on the low-angle side of the (005) reflection indicate the interstratification of other layer types (Figure 2). Accordingly, two structures were used to fit the experimental XRD pattern (Figure 5). The first one contains only 2W layers (layer thickness = 15.18 Å – Figure 5a – Table 3). This first periodic structure allows most features of the experimental XRD pattern to be reproduced, but the residual trace shows that the asymmetries described above were not reproduced (Figure 5a). A second contribution (60:30:10 ratio for 2W, 1W and 0W layers, respectively) was thus added. The XRD profile calculated for this additional MLS exhibits a (001) reflection shifted toward the high-angle side as compared to the pure 2W phase because of the presence of layers with lower layer thickness (0W, and 1W layers – Figure 5b). Mixing 87% of the first structure with 13% of the second allows the experimental pattern to be fitted satisfactorily ( $R_p = 1.45\%$  –

Figure 5c). The optimum fit to the experimental XRD patterns was obtained assuming for 2W layers the configuration of smectite interlayer species proposed by Ferrage *et al.* (2005a). This structure model includes a unique plane of H<sub>2</sub>O molecules located at 1.20 Å, along the c\* axis on either side of the interlayer mid-plane which contains exclusively interlayer Ca<sup>2+</sup> cations.

*Sample CaCl-SWy.* As compared to sample Ca-SWy, an increase of layer thickness for 2W layers and a decrease of layer thickness fluctuation ( $\sigma_z$ ) can be deduced from the qualitative description of the experimental XRD pattern recorded at 40% RH. Moreover, the extremely low value determined for the  $\xi$  parameter indicates an increased homogeneity of the hydration state. However, two structures were necessary to fit the experimental XRD pattern. These two structures differ from those obtained for sample Ca-SWy (Figure 6), as they both contain only 2W layers, differing only by their respective CSDSs (10.5 and 5.0 layers, respectively). This structural similarity arises from the discrepancies observed between the experimental pattern and the one calculated for the first 2W periodic structure which are symmetrical on each side of the calculated diffraction maxima (Figure 6a). Mixing the two contributions (80:20 ratio for the first and second periodic structures, respectively), leads to a satisfactory fit to the experimental pattern ( $R_p=3.70\%$  – Figure 6c – Table 3). In both structures, layer thickness of 2W layers is increased from 15.18 Å (sample Ca-SWy) to 15.295 Å (sample CaCl-SWy). The amount of interlayer H<sub>2</sub>O molecules is also increased from 2×3.2 (sample Ca-SWy) to 2×3.7 (Table 3 – Figure 6a). In addition, the  $\sigma_z$  parameter, corresponding to layer thickness fluctuation, is found now to be equal to zero, in agreement with the constant FWHM values determined for (00 $\ell$ ) reflections (Figure 3). To account for the increased intensity of the 002 reflection recorded for sample CaCl-SWy (as compared to sample Ca-SWy), the interlayer structure of 2W layers had to be modified from the model used to fit sample Ca-SWy. This model includes a central cation plane sandwiched between two planes of H<sub>2</sub>O molecules at a



distance of 1.2 Å along the  $c^*$  axis (Ferrage *et al.*, 2005a). For sample CaCl-SWy, the electron density had to be increased specifically in the interlayer mid-plane, where interlayer cations are located. Two models can give rise to such an increased electron density. In the first model, the scattering power of interlayer cations located in the interlayer mid-plane is increased, either by increasing their amount, with the strong constrain of the layer charge balance, or by increasing their specific scattering power. Both effects had to be combined to reproduce satisfactorily the experimental data. Accordingly, the optimum fit to the experimental XRD pattern of sample CaCl-SWy was obtained assuming for 2W layers the configuration of smectite interlayer species proposed by Ferrage *et al.* (2005a), and the sole presence of  $\text{CaCl}^+$  ion pairs in the interlayer mid-plane. Consistently, the number of monovalent  $\text{CaCl}^+$  ion pairs was twice that of  $\text{Ca}^{2+}$  in sample Ca-SWy. In the second model, additional neutral interlayer species, such as  $\text{H}_2\text{O}$  molecules for example, have to be introduced in the interlayer mid-plane in addition to interlayer  $\text{Ca}^{2+}$  cations, thus leading to a dramatically different interlayer structure. To fit the experimental data, the electron density in the interlayer mid-plane should be equivalent to that in the first model (presence of 0.72  $\text{CaCl}^+$  ion pairs per unit cell) and  $\sim 2.3$   $\text{H}_2\text{O}$  molecules should thus be present in this interlayer mid-plane in addition to  $\text{Ca}^{2+}$  cations (0.36 per unit cell). This second model is not consistent with the interlayer configuration refined by Ferrage *et al.* (2005c) for 2W smectite layers or with any alternative model from the literature and may thus be rejected. Modeling of XRD patterns recorded for Ca-SWy and CaCl-SWy samples thus provides unambiguous experimental support for the presence of  $\text{CaCl}^+$  ion pairs in Ca-saturated smectite samples prepared at high ionic strength.

*Smectite hydration in Ca- and CaCl-SWy samples*

In addition to the sole presence of  $\text{CaCl}^+$  ion pairs as interlayer cations in sample CaCl-SWy, XRD profile modeling highlighted significant differences in the hydration state of Ca- and CaCl-SWy samples. Specifically, at 40% RH, the latter sample contains only 2W layers (Figure 6 – Table 3), whereas different layer types are interstratified in the former sample. This increased homogeneity of hydration properties with increasing density of interlayer cations is reminiscent of the results obtained by Ferrage *et al.* (2005b) on two Ca-montmorillonites having contrasting layer charge deficits, and thus contrasting amounts of interlayer cations. To assess the stability of montmorillonite hydration properties as a function of RH, XRD patterns were recorded at 20% RH for both Ca- and CaCl-SWy samples (Figure 7). For sample Ca-SWy, the RH decrease results in a significant decrease of the  $d_{(001)}$  value corresponding to the transition from 2W to 1W layers (Figure 7), in a dramatic broadening of the (001) reflection and in a significant increase of the  $\xi$  parameter (1.30 Å). The experimental pattern obtained at 20% RH for sample Ca-SWy is similar to that obtained by Ferrage *et al.* (2005a), on the  $<1 \mu\text{m}$  size fraction of SWy-1 montmorillonite, thus implying similar proportions of the different layer types ( $\xi$  parameter near 1.24 Å and 45:40:15 ratio for 2W, 1W and 0W layers, respectively). On the other hand, only a limited shift of  $d_{(001)}$  is visible on the experimental XRD pattern obtained for sample CaCl-SWy at 20% RH as compared to that recorded at 40% RH. This shift is most probably related to the decrease of layer thickness for 2W layers with decreasing RH rather than to a significant heterogeneity of hydration properties, as no significant asymmetry is visible for  $(00\ell)$  reflections. This hypothesis is also supported by the similar low value (0.03 Å) determined for the  $\xi$  parameter at this lower RH value. The increased stability range of the bi-hydrated state towards the lower RH value observed for sample CaCl-SWy is consistent with the increased stability of this hydration state with increasing amount of interlayer cations reported by Ferrage *et al.* (2005b) for Ca-saturated montmorillonites.

This increased stability of the bi-hydrated state is accompanied at 40% RH by an increased amount of interlayer H<sub>2</sub>O molecules from 2×3.2 to 2×3.7 per unit cell for Ca- and CaCl-SWy samples, respectively (Table 3). NIR-DR spectra were recorded at 40% RH for these two samples to estimate the amount of interlayer H<sub>2</sub>O molecules (Figure 8). The combinations of stretching and bending modes are observed at 5250 and 5215 cm<sup>-1</sup> for Ca- and CaCl-SWy samples, respectively. Overtones of hydroxyl stretching modes from H<sub>2</sub>O molecules and structural OH groups are observed at 6830, 7095 cm<sup>-1</sup> and at 6805, 7065 cm<sup>-1</sup> for Ca- and CaCl-SWy samples, respectively. Over the two frequency ranges, the increased reflectance measured for sample CaCl-SWy as compared to sample Ca-SWy supports the higher amount of interlayer H<sub>2</sub>O molecules in the former sample although no quantitative estimate was performed. From NIR-DR results, the amount of H<sub>2</sub>O molecules in sample CaCl-SWy is sufficient to induce a network of H<sub>2</sub>O molecules similar to that in liquid H<sub>2</sub>O. In addition, profiles of NIR-DR spectra obtained for Ca- and CaCl-SWy samples are significantly different, the latter sample exhibiting a broad combination band as compared to sample Ca-SWy (Figure 8). This broadening is possibly related to the presence of Cl<sup>-</sup> anions that affects the local environment of adsorbed H<sub>2</sub>O molecules.

#### *Configuration of interlayer H<sub>2</sub>O molecules in Me- and MeCl-SWy samples*

NIR-DR spectroscopy was performed on out-gassed preparations of Ca- and CaCl-SWy samples (Figure 9) to study the configuration of the first hydration sphere around interlayer cations in these samples and to assess the possible influence of Cl<sup>-</sup> anions on the interaction between interlayer cation and H<sub>2</sub>O molecules. Even under deep-vacuum conditions, some H<sub>2</sub>O molecules bound to interlayer cations are still present, as shown by the combination of bending and stretching modes observed at 5240 and 5225 cm<sup>-1</sup> for out-gassed

Ca- and CaCl-SWy samples, respectively (Figure 9). These values may be assigned to strongly disturbed H<sub>2</sub>O molecules from the first hydration shell of interlayer cations. Bands observed at 6910, 7095 cm<sup>-1</sup> and at 6910, 7100 cm<sup>-1</sup> for out-gassed Ca- and CaCl-SWy samples, respectively, are assigned to the overtones of H<sub>2</sub>O molecules and layer hydroxyl stretching mode. From the comparison of the reflectance intensity measured on the combination bands, the amount of H<sub>2</sub>O molecules is clearly higher in sample Ca-SWy than in sample CaCl-SWy, although the amount of cations in the latter sample is presumably twice that in the former sample. This difference may be related to the local perturbation of the H<sub>2</sub>O-cation configuration because of the presence of Cl<sup>-</sup> anions modifying the affinity of Ca<sup>2+</sup> cations for H<sub>2</sub>O molecules. However, the profiles of the combination bands are rather similar for both samples.

From the qualitative observation of XRD patterns recorded for Me- and MeCl-samples, a peculiar behaviour was noted for sample MgCl-SWy (Table 2), this sample being the only one to show an increase of the  $\xi$  parameter from the Me- to the MeCl-sample (Table 2). This slight increase, which indicates a more heterogeneous structure for the MeCl-sample, can be related to the difficulty of Mg<sup>2+</sup> cations to exchange part of their H<sub>2</sub>O molecules for Cl<sup>-</sup>. The distribution of the H<sub>2</sub>O molecules in the first hydration shell of cations obtained from molecular dynamic simulations and wide angle neutron scattering data (Mazzarella *et al.*, 1967; Dickens and Brown, 1972; Hewish *et al.*, 1982; Spohr *et al.*, 1988) may provide some insight into the contrasting behaviour of Mg<sup>2+</sup> as compared to Ca<sup>2+</sup> or Sr<sup>2+</sup>. According to these results, Mg<sup>2+</sup> cations have a propensity to stick rigidly to a well-defined symmetrical octahedron, with low Mg-O(OH) distances, because of their high hydration energy. As a consequence, inner sphere MgCl<sup>+</sup> ion pairs are unlikely to form, although the increased intensity of the 002 reflection is consistent with the exclusive MgCl<sup>+</sup> ion pairs as interlayer cationic species (Figure 4). In contrast to Mg<sup>2+</sup>, Ca<sup>2+</sup> cations exhibit no regular symmetry in

their hydration shells, due to the weak hydration energy of  $\text{Ca}^{2+}$ .  $\text{Cl}^-$  anions therefore have an increasing tendency to replace  $\text{H}_2\text{O}$  molecules from the first hydration shell as one moves from  $\text{Mg}^{2+}$  to  $\text{Ca}^{2+}$  and  $\text{Sr}^{2+}$ . Accordingly, the  $\text{MgCl}^+$  ion pairs may not replace all  $\text{Mg}^{2+}$  cations in the interlayer of sample MgCl-SWy resulting in the coexistence of 2 types of 2W layers, one saturated by  $\text{Mg}^{2+}$  and the other by  $\text{MgCl}^+$  ions, thus increasing slightly the  $\xi$  parameter.

### *Smectite interlayer structure in Me- and MeCl-samples*

From XRD profile modeling results, the hypothesized presence of  $\text{CaCl}^+$  ion pairs, as compared to  $\text{Ca}^{2+}$  cations, in montmorillonite interlayers leads to significant differences for the CSDS, for layer thickness of 2W layers, and for the deviation from this modified layer thickness ( $\sigma_z$  – Table 3) in addition to the modified hydration properties described above. Ferrage *et al.* (2005a) have shown that the layer thickness depends on the cation ionic radius and on its affinity for  $\text{H}_2\text{O}$ . In the present study, layer thickness determined at 40% RH for 2W layers in sample Ca-SWy (15.18 Å) is close to that determined earlier (15.11 Å – Ferrage *et al.*, 2005a) whereas that determined for sample CaCl-SWy is considerably increased (15.295 Å). As Ferrage *et al.* (2005b) have shown that the interlayer cation density does not influence layer thickness at a given RH value on two montmorillonites with contrasting layer charges, the increased layer thickness is probably related to the presence of  $\text{Cl}^-$  (as  $\text{CaCl}^+$  ion pairs) rather than to the increased amount of Ca in the interlayer.

However, the increased amount of interlayer cations in sample CaCl-SWy as compared to sample Ca-SWy leads to an increase of the  $\text{H}_2\text{O}$  content (from  $2 \times 3.2$  to  $2 \times 3.7$  per unit cell, respectively – Table 3). The limited character of this associated increase is probably related to the almost complete filling of the interlayer space in sample CaCl-SWy. This

hypothesis is supported by the combined increase of the CSDS and decrease of the  $\sigma_z$  value (Table 3) which consistently indicate considerably lower layer thickness variability for 2W layers in sample CaCl-SWy. A possible cause of this decreased disorder in the montmorillonite structure is schematized in Figure 10. The incomplete interlayer filling of sample Ca-SWy may lead to a significant corrugation of the layers resulting from the local balance between attractive (between layer and interlayer cations) and repulsive (between adjacent layers) forces. In the proposed XRD modeling approach, this layer corrugation is accounted for by the  $\sigma_z$  parameter. For sample CaCl-SWy, the more complete filling of the interlayer space leads both to the increased layer thickness and to a more homogeneous distribution of interlayer species. As a result, local contrasts between interlayer domains containing or not interlayer cations are likely reduced, thus lowering the corrugation of the layers (Figure 10) and the fluctuation of layer thickness as observed experimentally.

Finally, the impact of the increased amount of interlayer species, and thus of the increased interlayer electron density, in MeCl-samples on the profiles of experimental XRD patterns may be used to assess the presence of such ion pairs. This ability is illustrated on Figure 4 by the linear correlation obtained between the scattering power of interlayer cationic species and the intensity of the (002) reflection measured experimentally. Consequently, this simple measurement can be used as a good indicator of the relative proportion of ion pairs present in the sample, provided that similar amounts of material are deposited on the oriented preparations for both Me- and MeCl-samples.

## CONCLUSIONS

The present study provides for the first time clear XRD experimental support for the presence of  $\text{MeCl}^+$  ion pairs in the interlayer of expandable clay minerals equilibrated with

high normality Me-Cl<sub>2</sub> solutions. This conclusion confirms the need to include these species in cation exchange thermodynamics calculations. Accordingly, Charlet and Tournassat (2005) have successfully modeled the interlayer composition of clay particles equilibrated with seawater, using for these species the exchange selectivity data reported by Tournassat *et al.* (2004b). However, the strong influence of these species in other salty environments may require further refinement of these preliminary parameters.

The possible introduction of MeCl<sup>+</sup> ion pairs in smectite interlayers is also of interest for the structural characterization of clay minerals because of the induced modifications of smectite hydration properties. For example, the multispecimen method developed initially by Drits *et al.* (1997a) and Sakharov *et al.* (1999) to characterize mixed-layer minerals requires fitting several experimental XRD patterns recorded for the same sample under different conditions, that is either with different interlayer cations and/or saturation with different polar molecules (H<sub>2</sub>O, ethylene glycol, ...) using a single structure model. As a result of these contrasting conditions, the behavior of expandable (smectite) layers is modified, thus providing additional constraints to the structure model. Because saturation of smectite interlayers with MeCl<sup>+</sup> ion pairs induces homogeneous hydration of the expandable layers, the number of parameters to be refined is thus reduced for each XRD pattern and a more reliable description of complex clay minerals can thus be obtained.

#### ACKNOWLEDGEMENTS

The results presented in the present article were collected during a Ph.D. thesis granted by ANDRA (French National Agency for Nuclear Waste Disposal). Andra is thanked for the permission to publish this manuscript and for financial support. The French Geological Survey (BRGM) is acknowledged for its editorial financial support. EF is grateful to Pr. Boris

A. Sakharov for fruitful discussions during XRD profile modeling. The manuscript was improved by the constructive reviews of two anonymous reviewers and AE David Laird, and by the remarks of Emmanuel Jacquot on an early version of the manuscript.

## REFERENCES

- Ben Brahim, J., Armagan, N., Besson, G. and Tchoubar, C. (1983) X-ray diffraction studies on the arrangement of water molecules in a smectite. I. Two-water-layer Na-beidellite. *Journal of Applied Crystallography*, **16**, 264-269.
- Ben Brahim, J., Besson, G. and Tchoubar, C. (1984) Etude des profils des bandes de diffraction X d'une beidellite-Na hydratée à deux couches d'eau. Détermination du mode d'empilement des feuillets et des sites occupés par l'eau. *Journal of Applied Crystallography*, **17**, 179-188.
- Bérend, I., Cases, J.M., François, M., Uriot, J.P., Michot, L.J., Masion, A. and Thomas, F. (1995) Mechanism of adsorption and desorption of water vapour by homoionic montmorillonites: 2. the  $\text{Li}^+$ ,  $\text{Na}^+$ ,  $\text{K}^+$ ,  $\text{Rb}^+$  and  $\text{Cs}^+$  exchanged forms. *Clays & Clay Minerals*, **43**, 324-336.
- Bishop, J., Murad, E. and Dyar, M.D. (2002) The influence of octahedral and tetrahedral cation substitution on the structure of smectites and serpentines as observed through infrared spectroscopy. *Clay Minerals*, **37**, 361-628.
- Bradley, W.F., Grim, R.E. and Clark, G.F. (1937) A study of the behavior of montmorillonite on wetting. *Zeitschrift Kristallographie*, **97**, 260-270.
- Burneau, A., Barrès, O., Gallas, J.P. and Lavalley, J.C. (1990) Comparative study of the surface hydroxyl groups of fumed and precipitated silicas. 2. Characterization by infrared spectroscopy of the interaction with water. *Langmuir*, **6**, 1364-1372.



- Burneau, A. and Carteret, C. (2000) Near infrared and ab initio study of the vibrational modes of isolated silanol on silica. *Physical Chemistry Chemical Physics*, **2**, 3217-3226.
- Cases, J.M., Bérend, I., François, M., Uriot, J.P., Michot, L.J. and Thomas, F. (1997) Mechanism of adsorption and desorption of water vapour by homoionic montmorillonite: 3. the  $Mg^{2+}$ ,  $Ca^{2+}$ ,  $Sr^{2+}$  and  $Ba^{2+}$  exchanged forms. *Clays & Clay Minerals*, **45**, 8-22.
- Charlet, L. and Tournassat, C. (2005) Fe(II)-Na(I)-Ca(II) cation exchange on montmorillonite in chloride medium; evidence for preferential clay adsorption of chloride – metal ion pairs in seawater. *Aquatic Geochemistry*, (Accepted).
- Cuadros, J. (1997) Interlayer cation effects on the hydration state of smectite. *American Journal of Science*, **297**, 829-841.
- Di Leo, P. and Cuadros, J. (2003) Cd-113, H-1 MAS NMR and FTIR analysis of  $Cd^{2+}$  adsorption on dioctahedral and trioctahedral smectite. *Clays and Clay Minerals*, **51**, 403-414.
- Di Leo, P. and O' Brien, P. (1999) Nuclear magnetic resonance (NMR) study of  $Cd^{2+}$  sorption on montmorillonite. *Clays and Clay Minerals*, **47**, 761-768.
- Dickens, B. and Brown, W.E. (1972) The crystal structure of  $CaKAsO_4 \cdot 8H_2O$ . *Acta Cryst.*, **B28**, 3056-3065.
- Drits, V.A. and Sakharov, B.A. (1976) *X-Ray structure analysis of mixed-layer minerals*. Dokl. Akad. Nauk SSSR, Moscow, 256 pp.
- Drits, V.A., Sakharov, B.A., Lindgreen, H. and Salyn, A. (1997a) Sequential structure transformation of illite-smectite-vermiculite during diagenesis of Upper Jurassic shales from the North Sea and Denmark. *Clay Minerals*, **32**, 351-371.

- Drits, V.A., Srodon, J. and Eberl, D.D. (1997b) XRD measurement of mean crystallite thickness of illite and illite/smectite: reappraisal of the kubler index and the scherrer equation. *Clays & Clay Minerals*, **45**, 461-475.
- Drits, V.A. and Tchoubar, C. (1990) *X-ray diffraction by disordered lamellar structures: Theory and applications to microdivided silicates and carbons*. Springer-Verlag, Berlin, 371 pp.
- Elprince, A.M., Vanselow, A.P. and Sposito, G. (1980) Heterovalent, ternary cation exchange equilibria:  $\text{NH}_4^+$ - $\text{Ba}^{2+}$ - $\text{La}^{3+}$  exchange on montmorillonite. *Soil Science Society of America Journal*, **44**, 964-969.
- Ferrage, E., Lanson, B., Sakharov, B.A. and Drits, V.A. (2005a) Investigation of smectite hydration properties by modeling of X-ray diffraction profiles. Part 1. Montmorillonite hydration properties. *American Mineralogist*, Ms #1776, in press.
- Ferrage, E., Lanson, B., Sakharov, B.A., Geoffroy, N. and Drits, V.A. (2005b) Investigation of smectite hydration properties by modeling of X-ray diffraction profiles. Part 2. Influence of layer charge and charge location. *American Mineralogist*, in preparation.
- Ferrage, E., Lanson, B., Malikova, N., Plançon, A., Sakharov, B.A. and Drits, V.A. (2005c) New insights on the distribution of interlayer water in bi-hydrated smectite from X-ray diffraction profile modeling of 00 $\ell$  reflections. *Chemistry of Materials*, Ms cm047995v, under review.
- Fletcher, P. and Sposito, G. (1989) The chemical modeling of clay/electrolyte interactions for montmorillonite. *Clay Minerals*, **24**, 375-391.
- Guinier, A. (1964) *Théorie et technique de la radiocristallographie*. Dunod, Paris, 740 pp.
- Hewish, N.A., Neilson, G.W. and Enderby, J. (1982) Environment of  $\text{Ca}^{2+}$  ions in aqueous solvent. *Nature*, **297**, 138-139.

- Howard, S.A. and Preston, K.D. (1989) Profile fitting of powder diffraction patterns. Pp. 217-275 in: *Modern Powder Diffraction* (D.L. Bish and J.E. Post, editors). Reviews in Mineralogy **20**, Mineralogical Society of America, Washington D.C.
- Hyun, S.P., Cho, Y.H., Kim, S.J. and Hahn, P.S. (2000) Cu(II) sorption mechanism on montmorillonite: an electron paramagnetic resonance study. *Journal of Colloid and Interface Science*, **222**, 254-261.
- Kittrick, J.A. (1969a) Interlayer forces in montmorillonite and vermiculite. *Soil Science Society of America Journal*, **33**, 217-222.
- Kittrick, J.A. (1969b) Quantitative evaluation of the strong-force model for expansion and contraction of vermiculite. *Soil Science Society of America Journal*, **33**, 222-225.
- Kodama, H., Gatineau, L. and Méring, J. (1971) An analysis of X-ray diffraction line profiles of microcrystalline muscovites. *Clays & Clay Minerals*, **19**, 405-413.
- Laird, D.A. (1996) Model for crystalline swelling of 2:1 phyllosilicates. *Clays & Clay Minerals*, **44**, 553-559.
- Laird, D.A. (1999) Layer charge influences on the hydration of expandable 2:1 phyllosilicates. *Clays & Clay Minerals*, **47**, 630-636.
- Madejova, J., Bujdak, J., Petit, S. and Komadel, P. (2000) Effects of chemical composition and temperature of heating on the infrared spectra of Li-saturated dioctahedral smectites. (II) Near-infrared region. *Clay Minerals*, **35**, 753-761.
- Mazzarella, L., Kovacs, A.L., De Santis, P. and Liquori, A.M. (1967) Three-dimensional X-ray analysis of the complex  $\text{CaBr}_2 \cdot 10\text{H}_2\text{O} \cdot 2(\text{CH}_2)_6\text{N}_4$ . *Acta Cryst.*, **22**, 65-74.
- Méring, J. (1949) L'interférence des rayons-X dans les systèmes à stratification désordonnée. *Acta Crystallographica*, **2**, 371-377.

- Mermut, A.R. and Lagaly, G. (2001) Baseline studies of the clay minerals society source clays: layer-charge determination and characteristics of those minerals containing 2:1 layers. *Clays and Clay Minerals*, **49**, 393-397.
- Mooney, R.W., Keenan, A.G. and Wood, L.A. (1952) Adsorption of water vapor by montmorillonite. II. Effect of exchangeable ions and lattice swelling as measured by X-ray diffraction. *Journal of American Chemical Society*, **74**, 1331-1374.
- Moore, D.M. and Reynolds, R.C., Jr (1997) *X-ray Diffraction and the Identification and Analysis of Clay Minerals*. Oxford University Press, Oxford and New York, 322pp pp.
- Nagelschmidt, G. (1936) The structure of montmorillonite. *Zeitschrift Kristallographie*, **93**, 481-487.
- Norrish, K. (1954) The swelling of montmorillonite. *Discussions of the Faraday society*, **18**, 120-134.
- Parkhurst, D.L. and Appelo, C.A.J. (1999) Phreeqc2 user's manual and program U.S. Geological Survey.
- Plançon, A. (2002) New modeling of X-ray diffraction by disordered lamellar structures, such as phyllosilicates. *American Mineralogist*, **87**, 1672-1677.
- Rhue, R.D. and Reve, W.H. (1990) Exchange capacity and adsorbed-cation charge as affected by chloride and perchlorate. *Soil Science Society of America Journal*, **54**, 705-708.
- Sakharov, B.A., Lindgreen, H., Salyn, A. and Drits, V.A. (1999) Determination of illite-smectite structures using multispecimen X-Ray diffraction profile fitting. *Clays & Clay Minerals*, **47**, 555-566.
- Schlegel, M., Manceau, A., Charlet, L. and Hazemann, J.L. (2001) Adsorption mechanisms of Zn on hectorite as a function of time, pH, and ionic strength. *American Journal of Science*, **301**, 798-830.

- Shainberg, I., Oster, J.D. and Wood, J.D. (1980) Sodium/calcium exchange in montmorillonite and Illite suspension. *Soil Science Society of America Journal*, **44**, 960-964.
- Spohr, E., Palinkas, G., Heinzinger, K., Bopp, P. and Probst, M.M. (1988) A molecular dynamics study of an aqueous SrCl<sub>2</sub> solution. *Journal of Physical Chemistry*, **92**, 6754.
- Sposito, G. (1977) The Gapon and Vanselow selectivity coefficients. *Soil Science Society of America Journal*, **41**, 1205-1206.
- Sposito, G. (1981) *The thermodynamics of soil solution*. Oxford University Press, New Yorkpp.
- Sposito, G. (1984) *Surface chemistry of soils*. Oxford University press, New York, 223 pp.
- Sposito, G. (1991) Effect of chloride on sodium-calcium and sodium-magnesium exchange on montmorillonite. *Soil Science Society of America Journal*, **55**, 965-967.
- Sposito, G., Holtzclaw, K.M., Charlet, L., Jouany, C. and Page, A.L. (1983a) Sodium-calcium and sodium-magnesium exchange on Wyoming bentonite in perchlorate and chloride background ionic media. *Soil Science Society of America Journal*, **47**, 51-56.
- Sposito, G., Holtzclaw, K.M., Johnston, C.T. and Le Vesque, C.S. (1981) Thermodynamics of sodium-copper exchange on Wyoming bentonite at 298 K. *Soil Science Society of America Journal*, **45**, 1079-1084.
- Sposito, G., Holtzclaw, K.M., Jouany, C. and Charlet, L. (1983b) Cation selectivity in sodium-calcium, sodium-magnesium, and calcium-magnesium exchange on Wyoming bentonite at 298 K. *Soil Science Society of America Journal*, **47**, 917-921.
- Stucki, J.W., Golden, D.C. and Roth, C.B. (1984) Effects of reduction and reoxidation of structural iron on the surface charge dissolution of dioctahedral smectites. *Clays & Clay Minerals*, **32**, 350-356.

- Suarez, D.L. and Zahow, M.F. (1989) Calcium-magnesium exchange selectivity of Wyoming montmorillonite in chloride, sulfate and perchlorate solutions. *Soil Science Society of America Journal*, **53**, 52-57.
- Tournassat, C., Ferrage, E., Poinsignon, C. and Charlet, L. (2004b) The titration of clay minerals. Part II. Structural-based model and implications for clay reactivity. *Journal of Colloid and Interface Science*, **273**, 238-250.
- Tournassat, C., Greneche, J.M., Tisserand, D. and Charlet, L. (2004a) The titration of clay minerals. Part I. Discontinuous backtitration technique combined to CEC measurements. *Journal of Colloid and Interface Science*, **273**, 228-237.
- Van Olphen, H. (1965) Thermodynamics of interlayer adsorption of water in clays. *Journal of Colloid Science*, **20**, 822-837.
- Vanselow, A.P. (1932a) Equilibria of the base-exchange reaction of bentonites, permutites, Soil colloids and zeolites. *Soil Science*, **33**, 95-113.
- Vanselow, A.P. (1932b) The utilization of the base-exchange reaction for the determination of activity coefficients in mixed electrolytes. *Journal of American Chemical Society*, **54**, 1307-1311.
- Vantelon, D., Pelletier, M., Michot, L.J., Barres, O. and Thomas, F. (2001) Fe, Mg and Al distribution in, the octahedral sheet of montmorillonites. An infrared study in the OH-bending region. *Clay Minerals*, **36**, 369-379.
- Walker, G.F. (1956) The mechanism of dehydration of Mg-vermiculite. *Clays & Clay Minerals*, **4**, 101-115.

**Table 1.** Cation exchange selectivity coefficients ( $K_v$ ) reported by Charlet and Tournassat (2005) for Na and Ca species including  $\text{CaCl}^+$  ion pairs.

| Exchange reaction  | $\log K_v$ |
|--|------------|
| $2 \text{NaX} + \text{Ca}^{2+} \Leftrightarrow \text{CaX}_2 + 2 \text{Na}^+$ | 0.4        |
| $\text{NaX} + \text{H}^+ \Leftrightarrow \text{HX} + \text{Na}^+$            | 0.0        |
| $\text{NaX} + \text{CaCl}^+ \Leftrightarrow \text{CaClX} + \text{Na}^+$      | 2.5        |

**Table 2.** Basal reflection qualitative descriptors (position and rationality) determined for Me- and MeCl-SWy samples (Me = Ca, Mg, Sr and Na) at 40% RH. The 001 reflection position ( $d_{(001)}$ ) is given in Å. The  $\xi$  parameter (in Å) which accounts for the departure from rationality of the  $00\ell$  reflection series is calculated as the standard deviation of the  $\ell \times d(00\ell)$  values calculated for the  $X_i$  measurable reflections over the  $2-50^\circ 2\theta$  Cu  $K\alpha$  angular range.

| Sample   | $d_{(001)}$ | $\xi / X_i$ |
|----------|-------------|-------------|
| Ca-SWy   | 15.23       | 0.15/5      |
| CaCl-SWy | 15.32       | 0.03/8      |
| Mg-SWy   | 15.03       | 0.09/5      |
| MgCl-SWy | 15.40       | 0.12/8      |
| Sr-SWy   | 15.40       | 0.09/5      |
| SrCl-SWy | 15.53       | 0.04/5      |
| Na-SWy   | 12.54       | 0.04/4      |
| NaCl-SWy | 12.54       | 0.04/4      |



**Table 3.** Optimum structural parameters used for the simulation of XRD profiles obtained for Ca- and CaCl-SWy samples. Both calculated patterns include the contributions of two structures (S). Layer Thickness (LT) of each layer type (2W, 1W, and 0W) is given in Å. Amounts of interlayer H<sub>2</sub>O molecules and cations are given per unit cell. N,  $\sigma^*$ , and  $\sigma_z$  indicate the size of the CSDs along the  $c^*$  axis, the deviation of particle orientation, and the fluctuation of layer thickness, respectively.

| Sample   | Ss Rel. Ab. | LT 2W  | LT 1W | LT 0W | N<br>(layers) | $\sigma^*$<br>(°) | $\sigma_z$<br>(Å) | Cations                | nH <sub>2</sub> O<br>2W | nH <sub>2</sub> O<br>1W |
|----------|-------------|--------|-------|-------|---------------|-------------------|-------------------|------------------------|-------------------------|-------------------------|
| Ca-SWy   | S1 – 87%    | 15.18  | -     | -     | 8.7           | 6.5               | 0.35              | 0.36 Ca <sup>2+</sup>  | 2×3.2                   | -                       |
|          | S2 – 13%    | 15.18  | 12.60 | 10.00 | 8.7           | 6.5               | 0.35              | 0.36 Ca <sup>2+</sup>  | 2×3.2                   | 3.6                     |
| CaCl-SWy | S1 – 80%    | 15.295 | -     | -     | 10.5          | 6.2               | 0.00              | 0.72 CaCl <sup>+</sup> | 2×3.7                   | -                       |
|          | S2 – 20%    | 15.295 | -     | -     | 5.0           | 6.2               | 0.00              | 0.72 CaCl <sup>+</sup> | 2×3.7                   | -                       |

## FIGURE CAPTION

**Figure 1.** Calculated cationic composition of smectite interlayers as a function of ionic strength in a  $\text{CaCl}_2$  ionic background. Simulation parameters are listed in Table 1. Solid line: sorbed amount of  $\text{Ca}^{2+}$  in  $\text{mol.kg}^{-1}$ . Dotted line: sorbed amount of  $\text{CaCl}^+$  in  $\text{mol.kg}^{-1}$ . The gray bar indicates the 1 M  $\text{CaCl}_2$  ionic background used for preparation of sample CaCl-SWy. The open bar indicates the low ionic strength conditions used for preparation of sample Ca-SWy

**Figure 2.** Experimental XRD patterns obtained for Me- and MeCl-samples. **(a)** Me = Ca, Mg, and Sr. **(b)** Me = Na. Intensities in the high-angle region ( $8-50^\circ 2\theta$ ) are scaled up ( $\times 15$  in **a** and  $\times 5$  in **b**). (002) and (007) and (008) reflections are zoomed up for Ca- and CaCl-SWy samples. Quartz,  $\text{SrCl}_2$  and NaCl impurities are marked as Qz, † and \*, respectively.

**Figure 3.** Evolution of the full width at half maximum intensity (FWHM) measured on (00 $\ell$ ) basal reflection as a function of the  $\ell$  index for Me- and MeCl-SWy samples (solid and dashed lines, respectively – Me = Ca, Mg, Sr and Na).

**Figure 4.** Intensity ratio of (002) reflections measured on MeCl- and Me-SWy XRD patterns as a function of the scattering factor ratio ( $\eta$ ) between  $\text{MeCl}^+$  and  $\text{Me}^{2+}$  interlayer species (Me = Ca, Mg or Sr), weighted for their valency (see text for details).

**Figure 5.** Modeling of XRD patterns recorded at 40% RH for sample Ca-SWy. Grey bar indicates the scaling up ( $\times 10$ ) of the high-angle region intensities. Experimental pattern is shown as crosses whereas calculated patterns and difference plots are shown as solid lines. **(a)** XRD pattern calculated for a pure bi-hydrated periodic structure. **(b)** XRD pattern calculated for a MLS structure containing 60%, 30% and 10% of 2W, 1W and

0W, respectively. (c) Optimum fit to the experimental pattern, corresponding to the combination of the above two structures in a 87:13 ratio.

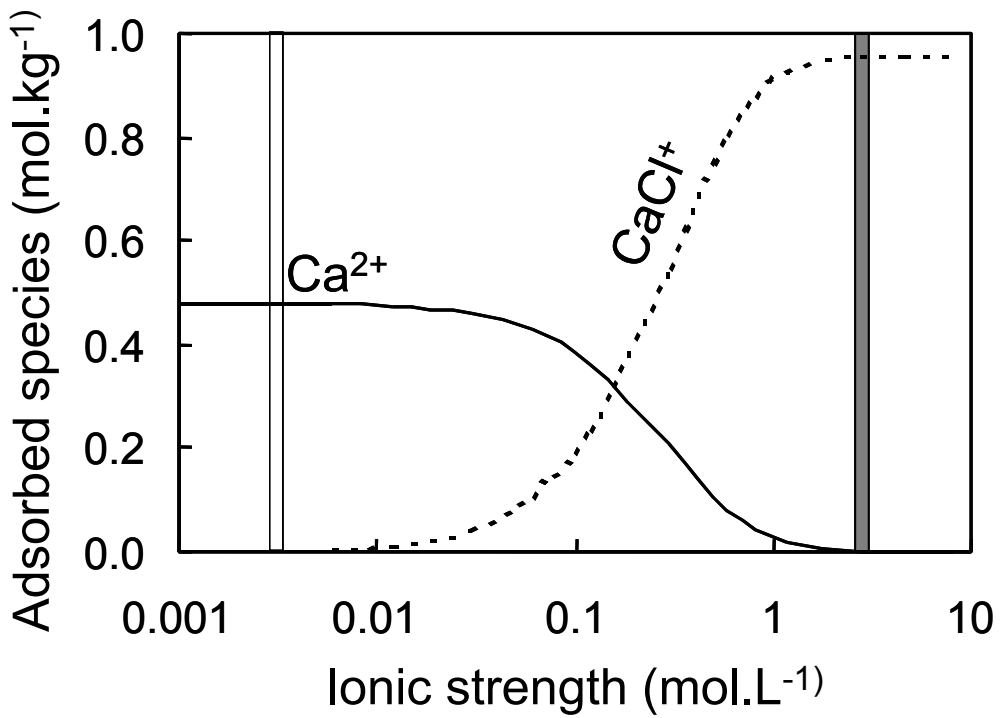
**Figure 6.** Modeling of XRD patterns recorded at 40% RH for sample CaCl-SWy. Patterns as Fig. 5. (a) XRD pattern calculated for a pure bi-hydrated structure with an average CSDS along the  $c^*$  axis of 10.5 layers. (b) XRD pattern calculated for a pure bi-hydrated periodic structure with an average CSDS along the  $c^*$  axis of 5.0 layers. (c) Optimum fit to the experimental pattern, corresponding to the combination of the above two structures in a 80:20 ratio.

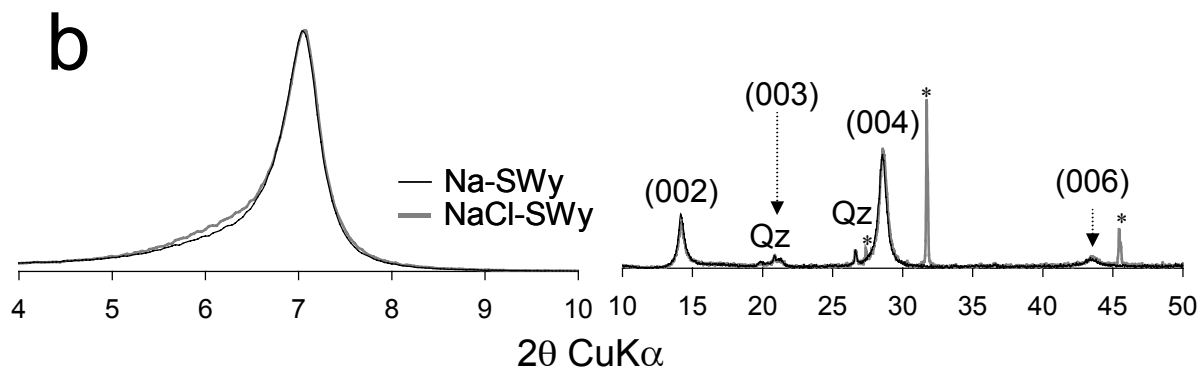
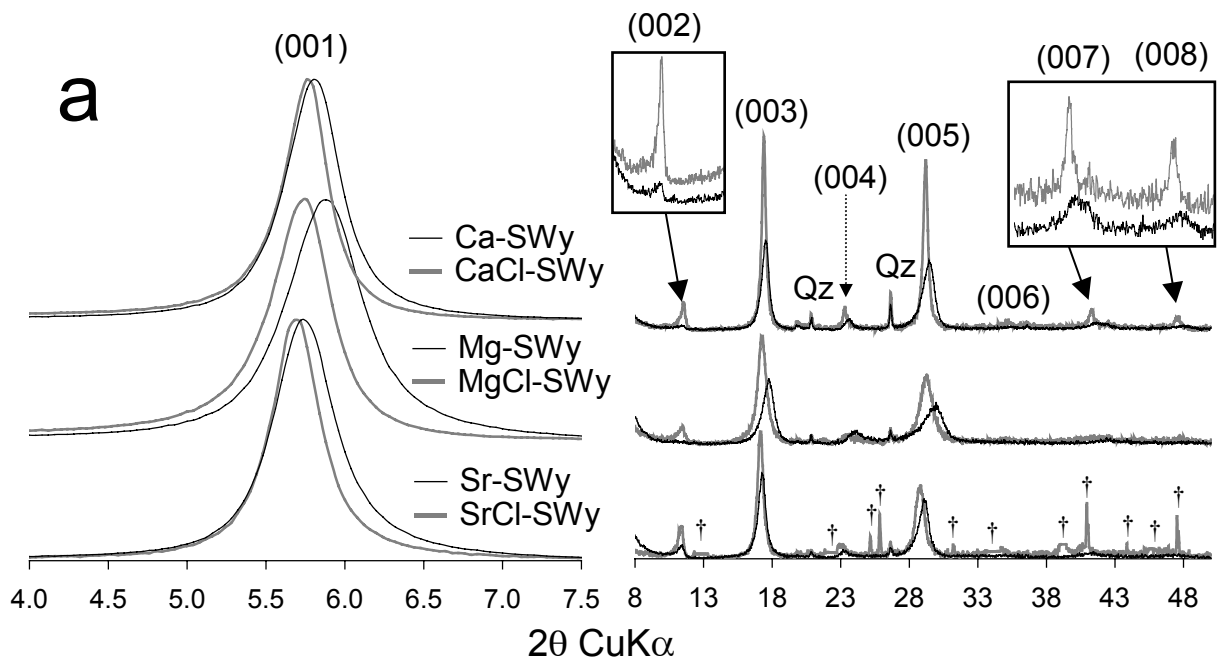
**Figure 7.** Comparison of experimental XRD patterns recorded for Ca- and CaCl-SWy samples at 40 and 20% RH. Intensities in the high-angle region ( $8-50^\circ 2\theta$ ) are scaled up ( $\times 15$ ) in comparison to the low-angle region.

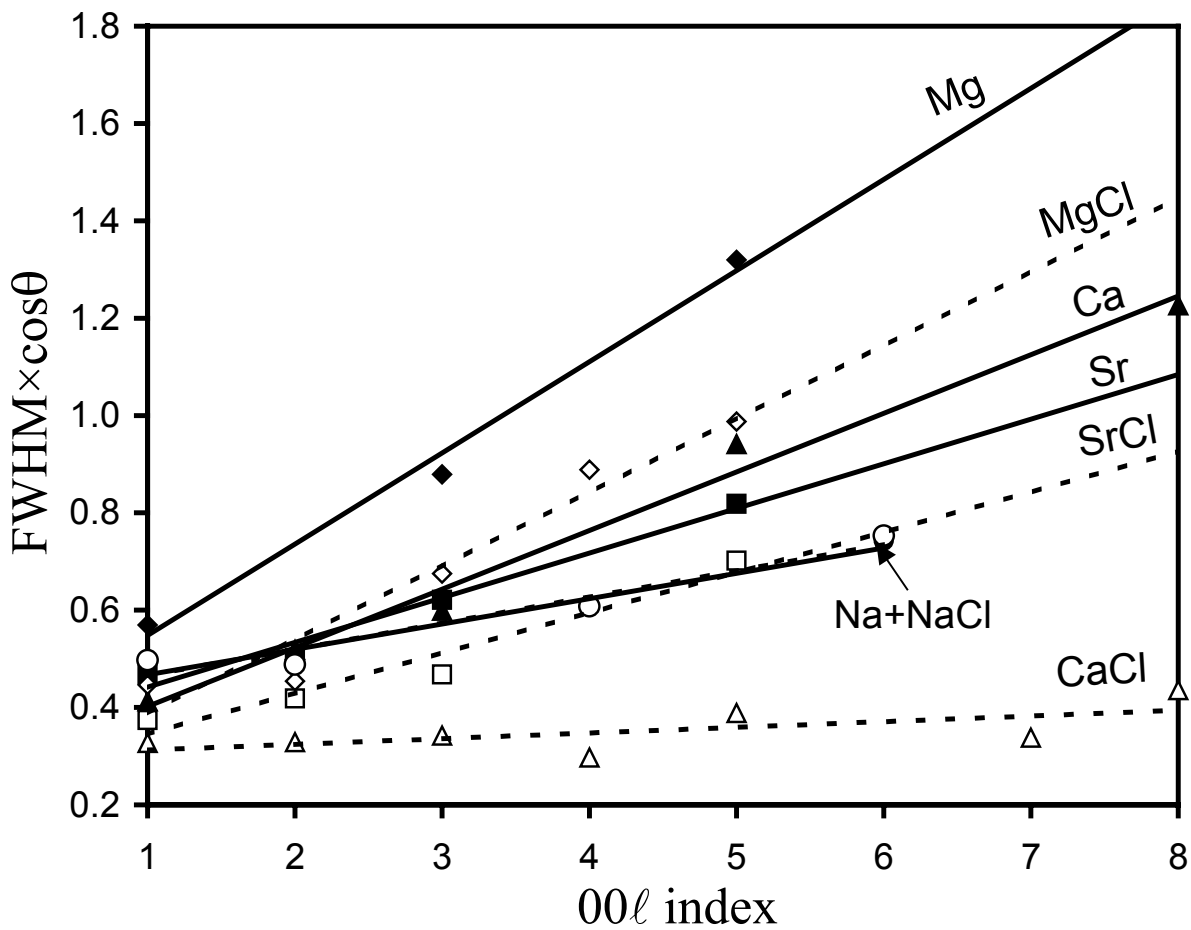
**Figure 8.** NIR-DRS spectra of Ca- and CaCl-SWy at 40 % RH. Solid and dashed lines represent Ca- and CaCl-SWy samples respectively.

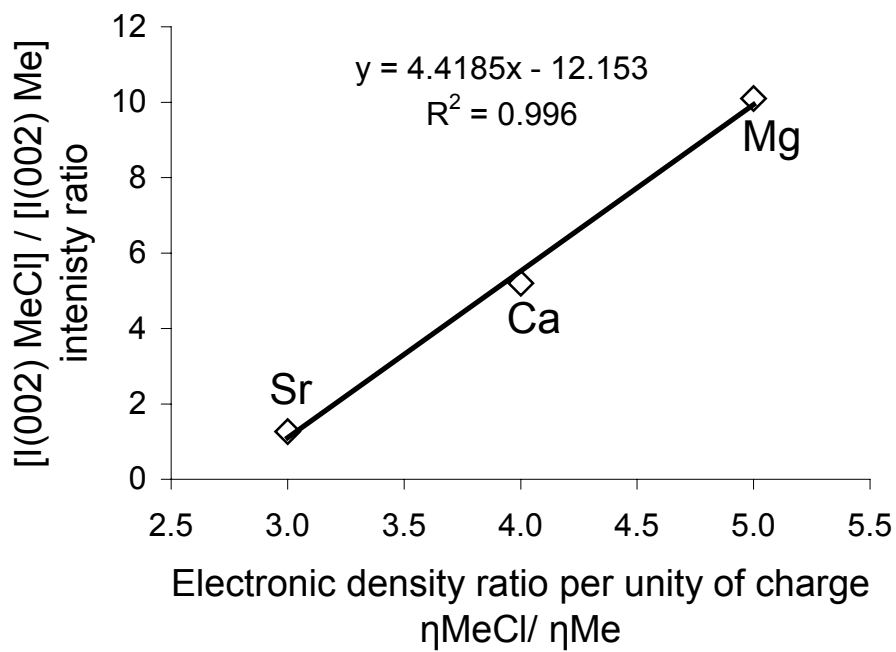
**Figure 9.** NIR-DRS spectra of out-gassed Ca- and CaCl-SWy. Patterns as Fig. 8.

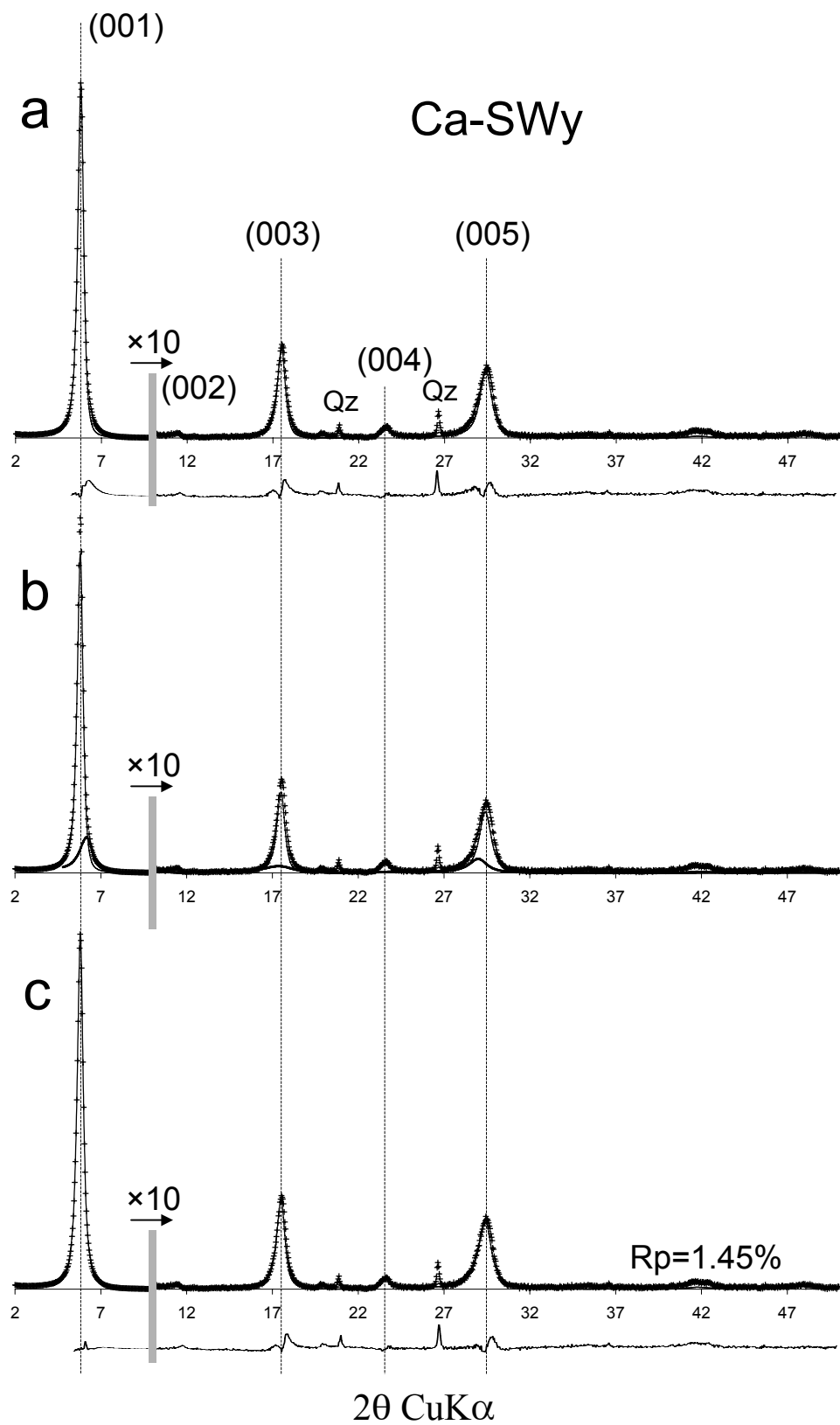
**Figure 10.** Schematic representation of the influence of  $\text{MeCl}^+$  ion pairs in smectite interlayers. The incomplete interlayer filling of sample Ca-SWy (left) leads to a significant corrugation of the layers resulting from the local balance between attractive (between layer and interlayer cations) and repulsive (between adjacent layers) forces. For sample CaCl-SWy (right), the more complete filling of the interlayer space leads both to the increased layer thickness and to a more homogeneous distribution of interlayer species, thus lowering the corrugation of the layers and the fluctuation of layer thickness.



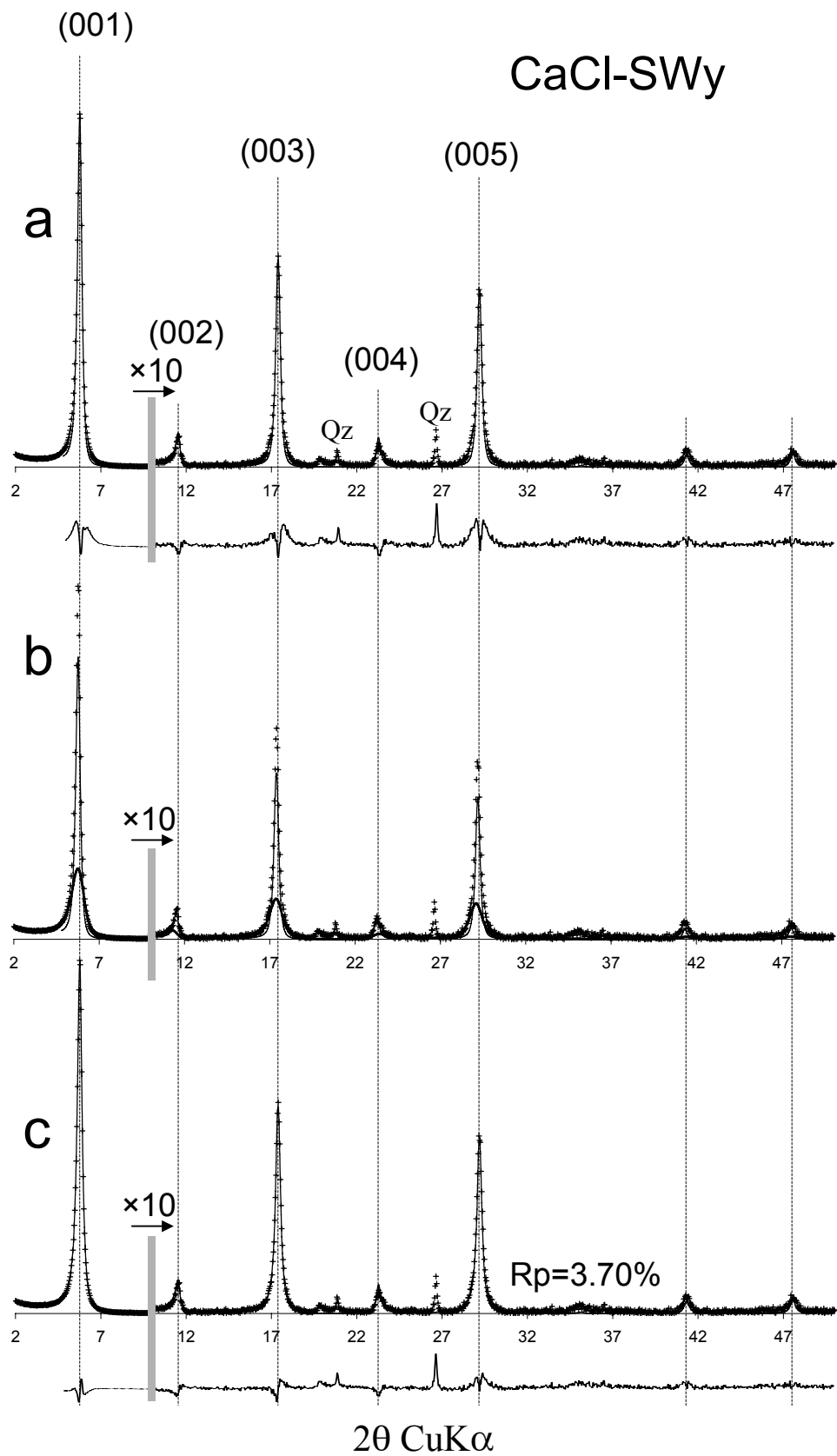




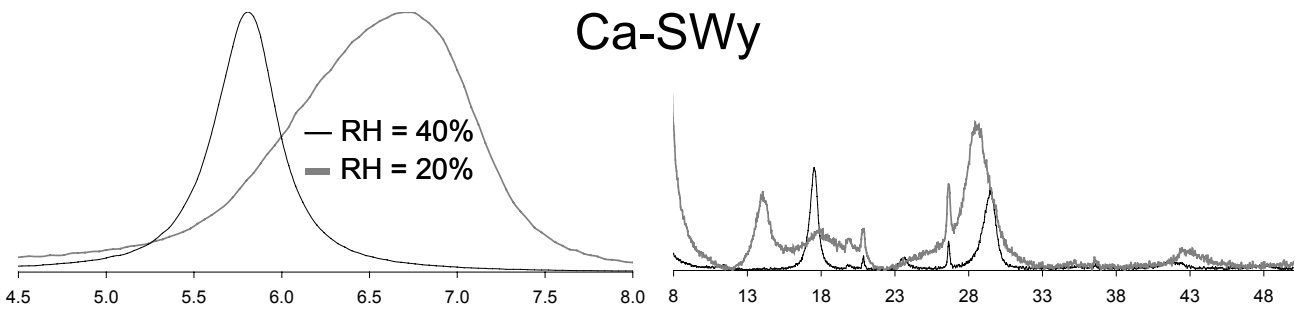




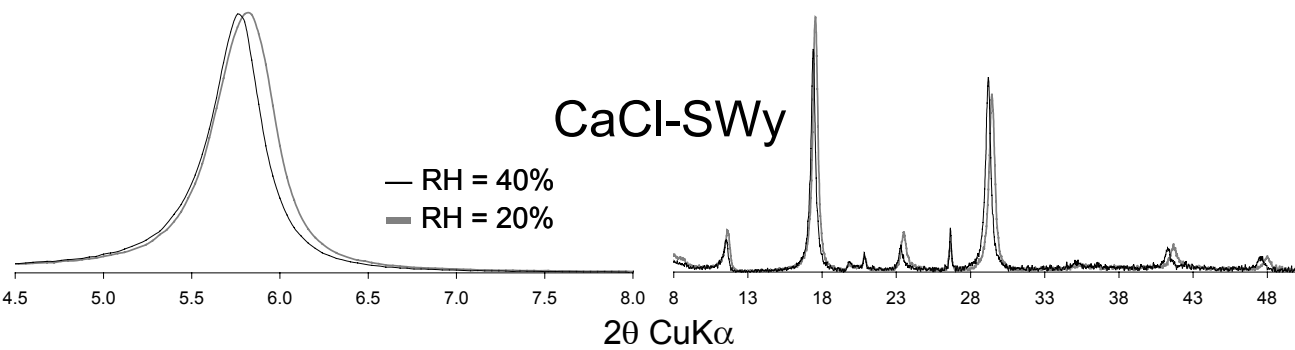


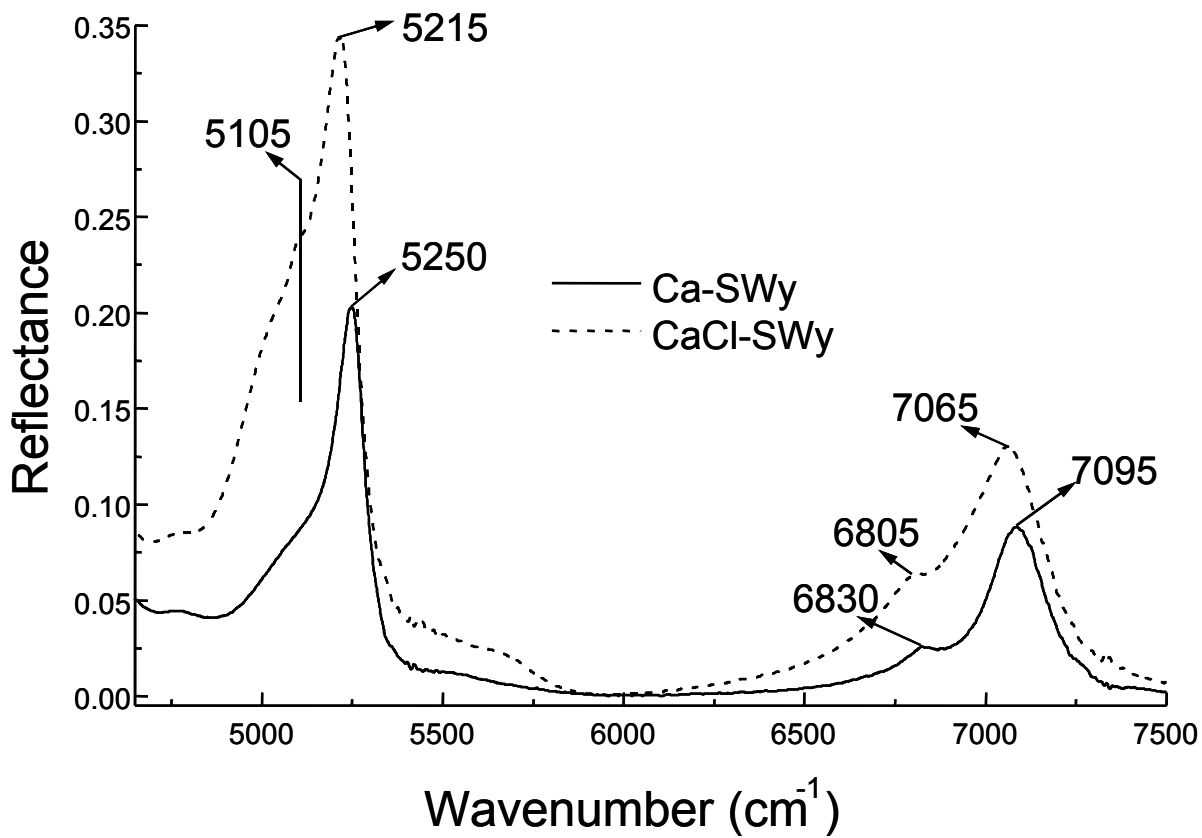


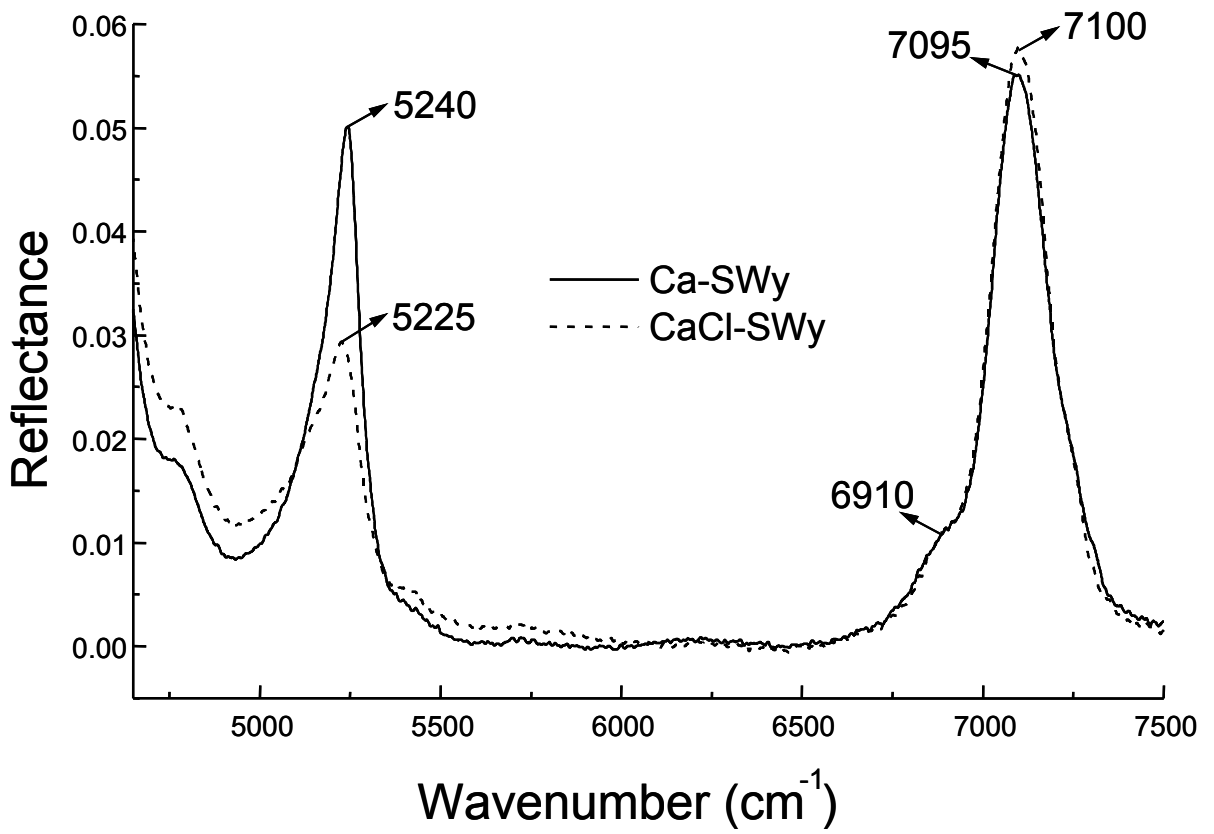
### Ca-SWy



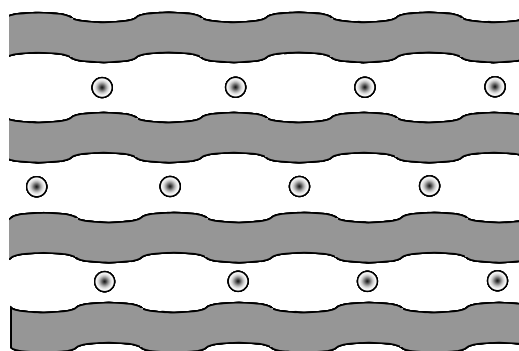
### CaCl-SWy







Ca-SWy



CaCl-SWy

